Ultramicroscopy 236 (2022) 113493

Contents lists available at ScienceDirect

Ultramicroscopy

journal homepage: www.elsevier.com/locate/ultramic

AutomAl 6000: Semi-automatic structural labelling of HAADF-STEM images of precipitates in Al–Mg–Si(–Cu) alloys

Haakon Tvedt [a,*], Calin D. Marioara [b], Elisabeth Thronsen [a], Christoph Hell [a], Sigmund J. Andersen [b], Randi Holmestad [a]

[a] Department of Physics, Norwegian University of Science and Technology (NTNU), Høgskoleringen 5, Trondheim, N-7491, Norway
[b] Materials and Nanotechnology Department, SINTEF Industry, Høgskoleringen 5, Trondheim, N-7465, Norway

ARTICLE INFO

Keywords:
HAADF-STEM
Aluminium
Al–Mg–Si(–Cu) alloys
Precipitate
AutomAl 6000
Algorithm

ABSTRACT

When the Al–Mg–Si(–Cu) alloy system is subjected to age hardening, different types of precipitates nucleate depending on the composition and thermomechanical treatment. The main hardening precipitates extend as needles, laths or rods along the <100> directions in the aluminium matrix. It has been found that the structures of all metastable precipitates may be generalized as stacks of <100> columns, where most of these columns are replaced by solute elements. In the precipitates, a column relates to neighbour columns by a set of simple structural principles, which allows identification of species and relative longitudinal displacement over the (100) cross-section.

Aberration-corrected high-angle annular dark field scanning transmission electron microscopy (HAADF-STEM) is an important tool for studying such precipitates. With the goal of analysing atomic resolution HAADF-STEM images of precipitate cross-sections in the Al–Mg–Si(–Cu) system, we have developed the stand-alone software AutomAl 6000, which features a column characterization algorithm based on the symbiosis of a statistical model and the structural principles formulated in a digraph-like framework. The software can semi-autonomously determine the 3D column positions in the image, as well as column species. In turn, AutomAl 6000 can then display, analyse and/or export the structure data.

This paper describes the methodology of AutomAl 6000 and applies it on three different HAADF-STEM images, which demonstrate the methodology. The software, as well as other resources, are available at http://automal.org. The source code is also directly available from https://github.com/Haawk666/AutomAl-6000.

1. Introduction and background

Aberration-corrected high-angle annular dark field scanning transmission electron microscopy (HAADF-STEM) can achieve atomic resolution of the nano-scale structure of crystal materials [1,2]. AutomAl 6000 is a new software tool for analysing HAADF-STEM images of precipitates in the Al–Mg–Si(–Cu) alloy system. These alloys are important light weight materials with increased use [3–8]. Their properties depend strongly on the precipitates, which means there is an increasing demand for more precise quantification of the micro- and nano-structure. For atomically resolved images oriented along one of the <100> Al directions, the software maps the atomic structure of precipitates embedded in the Al matrix. In the following, the direction into the image will be taken as [001]Al. In this work, we discuss the structural arrangement principles in the Al–Mg–Si(–Cu) precipitates and develop a column characterization algorithm from these principles by using statistics and graph theory. This enables identification of the atomic species (Al, Mg, Si or Cu) and longitudinal displacement ($z = 0$ or $z = \frac{1}{2}a_{\mathrm{Al}}$ in terms of the heights of the two planes in the Al cell, with lattice constant $a_{\mathrm{Al}} = 4.05$ Å [9]). By determining all column heights and positions, the atomic structure over the entire image can be mapped. This data can then be exported as *scalable vector graphics* (SVG) to produce high quality atomic overlays with SVG software, or as raw data in *comma separated values* (CSV) format, which can then be parsed for other uses.

This paper is focused on the underlying theory and principles used to develop the column characterization algorithm, which is the main feature and novelty of the AutomAl 6000 software. Implementation details are mostly avoided. However, successful user deployment of the algorithm mainly depend on the user's ability to interpret and correct the resulting atomic graphs. This technique is briefly described in the results and discussion section, but readers who are interested in practical application of the software, are encouraged to instead follow

* Corresponding author.
E-mail address: haakon.tvedt@ntnu.no (H. Tvedt).

https://doi.org/10.1016/j.ultramic.2022.113493
Received 14 September 2021; Received in revised form 11 January 2022; Accepted 15 February 2022
Available online 10 March 2022
0304-3991/© 2022 The Authors. Published by Elsevier B.V. This is an open access article under the CC BY license (http://creativecommons.org/licenses/by/4.0/).

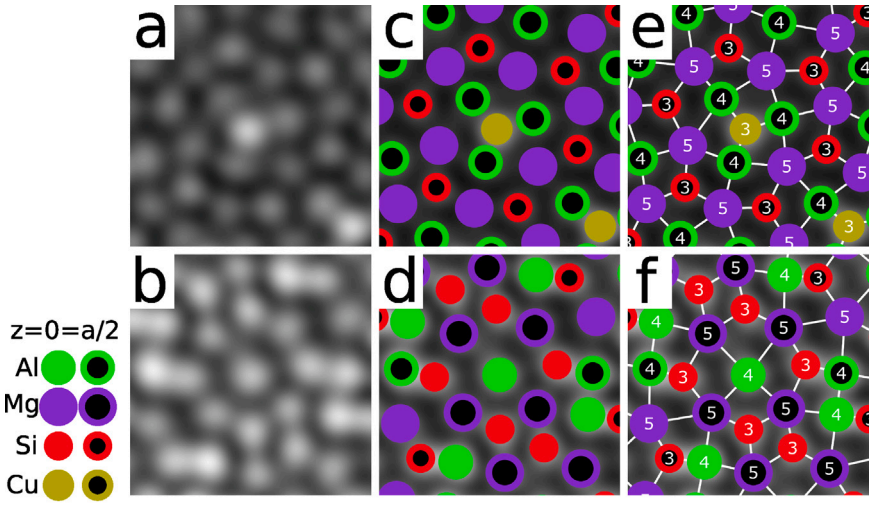

Fig. 1. Structural principles in Al-Mg-Si-(Cu) precipitates. Black and coloured centres show the two normal plane heights of the precipitate columns (associated with the parallel <100> columns of the surrounding matrix). The principles relate the atomic species to its OPNN quantity. Excerpts of HAADF-STEM images are given of two precipitates: (a) β'_{Cu} and (b) β''. The respective atomic overlays are shown in (c) and (d), and the number of OPNN (connected by white lines) are indicated in (e) and (f).

the "quickstart" tutorial video, which is linked on the web-page. The tutorial offers a more practical introduction to the atomic graph review process, as well as other important aspects of the software that are not covered here.

1.1. Column arrangement principles

In the FCC Al matrix, neighbour (001) planes are separated by 2.025 Å. As a consequence of their 3D stacking, a <001> column is relatively shifted compared to its neighbouring columns by half a unit cell in the z-direction. One can therefore associate all atom columns with one of two relative heights: $z = 0$ or $z = \frac{1}{2}a_{\mathrm{Al}}$. For an atom on one plane, 1/3 of the nearest neighbours (NN) is on the same plane, the rest on the two opposite planes.

The NN arrangement around a column depends on its majority element and follows a set of simple principles. This allows identification of column species and height: Al keeps the 4-fold FCC arrangement with 12 NN. This means an Al column is always surrounded by 4 NN associated with the same plane and two sets of 4 opposite plane NN (OPNN). The Mg atoms favour 15 NN (or 5 OPNN), and the smaller Cu and Si atoms favour 9 NN (or 3 OPNN) [10].

Fig. 1 illustrates the structural principles in two fragments of common Al–Mg–Si(–Cu) precipitate phases. Fig. 1a shows an excerpt of a β'_{Cu} phase, while 1b shows an excerpt from a β'' phase [4,5]. The corresponding atomic overlays are shown in Figs. 1c and 1d. According to the structural principles, Al has 4 OPNN, while Mg has 5 OPNN, and both Si and Cu have 3 OPNN. This is visualized in Figs. 1e and 1f, where the number of OPNN is indicated by the white lines radiating from/connected to an atom. Si and Cu, which both occupy 3 OPNN positions, are distinguished by Z-contrast.

There are some exceptions to these principles, for instance the central Si column of β' with its higher occupancy, which undermines the opposite plane dichotomy [11]. Despite β' and other exceptions, these principles are useful for determining structure and interfaces in most Al–Mg–Si(–Cu) precipitates, including hybrid precipitates and/or disordered precipitates [4,5].

1.2. Statistical modelling

To build statistical models which can infer the atomic species of columns, a *multivariate normal distribution* scheme is applied [12]. Define a set of N data points $\{\boldsymbol{x}_n\}$ with K numerical attributes[1] such that

$$\boldsymbol{x}_n = [x_{n1},\ x_{n2},\ \ldots,\ x_{nk},\ \ldots,\ x_{nK}]^T, \tag{1}$$

where T is the transposition operator. The means are calculated as $\boldsymbol{\mu} = [\mu_1,\ \mu_2,\ \ldots,\ \mu_k,\ \ldots,\ \mu_K]$, where

$$\mu_k = \frac{1}{N}\sum_{n=1}^{N} x_{nk}. \tag{2}$$

This gives the $K \times K$ covariance matrix $\boldsymbol{\Sigma}$, with elements

$$\Sigma_{kh} = \frac{1}{N-1}\sum_{n=1}^{N}(x_{nk} - \mu_k)(x_{nh} - \mu_h). \tag{3}$$

The multivariate normal distribution f of the given data can now be expressed as

$$f(\boldsymbol{x} \mid \boldsymbol{\mu},\ \boldsymbol{\Sigma}) = (2\pi)^{-\frac{K}{2}}|\boldsymbol{\Sigma}|^{-\frac{1}{2}} \cdot \exp\left[-\frac{1}{2}(\boldsymbol{x}-\boldsymbol{\mu})^T\boldsymbol{\Sigma}^{-1}(\boldsymbol{x}-\boldsymbol{\mu})\right], \tag{4}$$

where $|\boldsymbol{\Sigma}|$ is the determinant of the covariance matrix, and $\boldsymbol{\Sigma}^{-1}$ is the inverse covariance matrix. If the data, in addition to its numerical attributes, is also grouped in a finite discrete nominal attribute $s \in \{s_1,\ s_2,\ \ldots,\ s_l,\ \ldots,\ s_L\}$ with L categories, then each category will have an associated distribution $f_l(\boldsymbol{x} \mid \boldsymbol{\mu}_l,\ \boldsymbol{\Sigma}_l)$. The *category probability vector* P of a new data point $\boldsymbol{y} = [y_1,\ y_2,\ \ldots,\ y_k,\ \ldots,\ y_K]^T$ has elements

$$P_l = \left(\sum_{m=1}^{L} f_m(\boldsymbol{y})\right)^{-1} f_l(\boldsymbol{y}), \tag{5}$$

where P_l is the probability that $\boldsymbol{y}$ belongs in category s_l.

1.3. Digraphs

In graph theory, a *simple digraph* G is a particular class of graphs, where a set of *vertices* $\{v_i\}$, also called the *vertex set* $V(G)$, is connected by a set of unique *directed arcs* $\{a_j = v_k v_l \neq v_l v_k\}$, also called the *arc set*

[1] *Numerical attributes* are typically real-valued variables, like Z-contrast or temperature. In contrast, *nominal attributes* are categorical variables, like atomic species or cities.

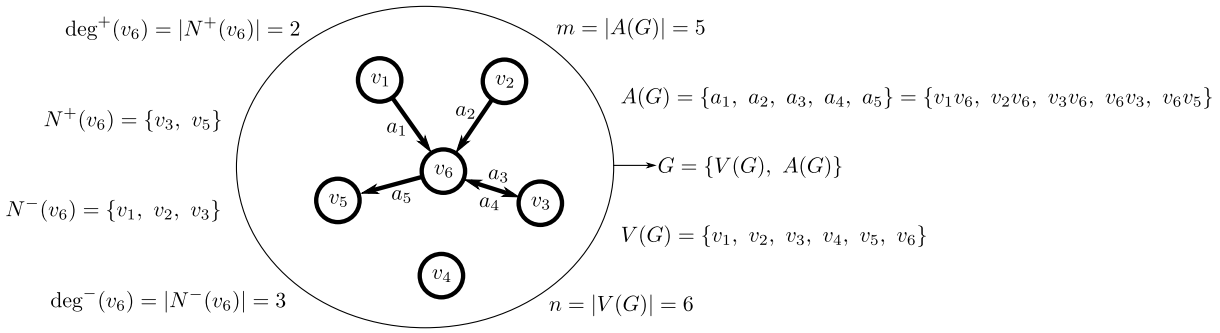

Fig. 2. Digraph nomenclature. Consider an example digraph G. On the right is the complete set description of the graph, which defines the digraph G, with vertex set $V(G)$, arc set $A(G)$, order n and size m. On the left is the in- and out-neighbourhood of vertex v_6, with the corresponding vertex in- and out-degree. Note also, that the arcs $a_3 = v_3v_6$ and $a_4 = v_6v_3$ are symmetric, with a_3 being the inverse of a_4 and *vice versa*. The arcs $a_1 = v_1v_6$, $a_2 = v_2v_6$ and $a_5 = v_6v_5$, are all un-symmetric because they have no inverse counterpart. In this example, vertex v_4 is disconnected from the rest of the graph.

$A(G)$, with the restriction $k \neq l$, see for instance [13]. Consider Fig. 2, which illustrates the digraph nomenclature presented in this section. If the arc v_kv_l is in the arc set of a graph $A(G)$, then v_k is *adjacent to* v_l, and v_l is *adjacent from* v_k. v_l is also the *out-neighbour* of v_k. The set of all out-neighbours of a vertex v_i is termed the *out-neighbourhood* of v_i, notated $N^+(v_i)$. The *out-degree* of a vertex v_i is equal to the cardinality of the out-neighbourhood of the vertex,

$$\deg^+(v_i) = |N^+(v_i)|. \tag{6}$$

An analogous nomenclature for in-neighbourhoods is achieved by replacing the superscript plus sign with a minus sign. The more general *neighbourhood* of v_i is the union of its in- and out-neighbourhoods, $N(v_i) = N^+(v_i) \cup N^-(v_i)$. The inverse of the arc v_kv_l is the arc v_lv_k. If the inverse arc of a_j is in the arc set, then both a_j and its inverse are *symmetric*. If all the arcs in $A(G)$ are symmetric, then G is symmetric. The *size* m of a digraph G is the number of arcs in its arc set $m = |A(G)|$, while the *order* n of the graph, is the number of vertices in its vertex set $n = |V(G)|$. Small local graph permutations are sometimes referred to as *graph edits*, like for instance removing an arc from the arc set $A(G)$.

2. Method

Based on digraphs, a framework termed *atomic graphs* was developed and implemented as the data-structure for AutomAl 6000, see below. Fig. 3 shows the overall AutomAl 6000 workflow: After a proper column detection has been achieved, either by using *Atomap* [14], or by performing appropriate pre-processing followed by the column detection routine of AutomAl 6000, the column characterization algorithm can be applied. This algorithm combines several sub-methods which are explored later in this section. Once column characterization is completed, manual review of the results is supported by the digraph interface of AutomAl 6000, which is further discussed in the results and discussion section.

2.1. Atomic graphs

Adding selected key properties and restrictions to simple digraphs, enabled the design of a flexible and 'algorithm friendly' framework for modelling OPNN structures, termed *atomic graphs*. Here, each vertex v_i has a spatial position (x_i, y_i, z_i). The opposite plane dichotomy is modelled with a Boolean value

$$\zeta_i = \frac{2}{a_{\mathrm{Al}}} z_i \qquad \in \{0,\ 1\}. \tag{7}$$

It is also convenient to define the *partners* P of a vertex v_i as the intersection of the in- and out-neighbourhood of the vertex

$$P(v_i) = N^+(v_i) \cap N^-(v_i), \tag{8}$$

which thus contains all neighbours connected by symmetric arcs. Let the *symmetric degree* of a vertex v_i be

$$\deg^{\leftrightarrow}(v_i) = |P(v_i)|. \tag{9}$$

Notice that in Fig. 2, $P(v_6) = \{v_3\} \Rightarrow \deg^{\leftrightarrow}(v_6) = 1$, since only one vertex (v_3) is in both $N^+(v_6)$ and $N^-(v_6)$. Additionally, given the spatial property of the vertices, arcs in atomic graphs cannot intersect in the 2D projection of the graph. Fig. 4 shows the atomic graph of a single β'' molecule embedded in the aluminium matrix (right). Also in Fig. 4, some vertex degrees and arcs are erroneous with regards to the OPNN structure of the same unit of β'' (left) [5].

If a graph is sparse, which means that the average vertex degree is much less than the order of the graph, then the preferred method of implementation of its data-structure is an *adjacency list* [17]. With this method, each vertex is an object which stores a list of all its out-neighbours. This is a convenient structure for certain graph-traversal algorithms like *depth first search* [17], and is the method of implementation of atomic graphs in AutomAl 6000, which indeed are sparse.

The strength of the digraph-like formulation, is that a graph can now be moulded by using a set of four basic graph edits: (1) *arc pivot* $\hat{P}_{ijk}(G)$, which deletes the arc v_iv_j, assuming it exists, and creates the arc v_iv_k, assuming it does not already exist; (2–3) *degree increment* $\hat{D}_i^+(G)$ and *degree decrement* $\hat{D}_i^-(G)$, which will alter the out-degree of vertex v_i and thus consequently create or delete an arc, respectively; and (4) *plane inversion* $\hat{I}_i(G)$, which will invert the plane association (the ζ_i value) of vertex v_i.

Arc pivot and plane inversion are *weak* permutations, because they will not alter vertex degrees, while vertex increment and vertex decrement are *strong* permutations, because they will alter vertex degrees. For clarity, the effects of the edits discussed above are illustrated in Fig. 4.

There is also a second level of abstraction with an additional set of four conditional edits used by the algorithm. These edits attempt to implement a preliminary logic before deciding to apply the more basic edits of the previous paragraph. In brief, these edits are: (1) *strong arc preservation* $\hat{S}_{ij}^+(G)$, which will apply $\hat{D}_j^+(G)$ if possible, and if so, create the arc v_jv_i; (2) *strong arc termination* $\hat{S}_{ij}^-(G)$, which will apply $\hat{D}_i^-(G)$ if possible, and if so delete the arc v_iv_j; (3) *weak arc preservation* $\widehat{W}_{ij}^+$, which will look for a suitable vertex v_k and perform $\hat{P}_{ikj}(G)$ if possible; and (4) *weak arc termination* $\widehat{W}_{ij}^-(G)$, which will look for a suitable vertex v_l and perform $\hat{P}_{ijl}(G)$ if possible.

Fig. 4 provides an example graph edit sequence $\hat{T}$ that optimizes the symmetry of the atomic graph. Table 1 provides a summary of the graph edits. The goal of any graph edit is to converge towards the actual OPNN structure of the precipitate.

If the column arrangement principles hold throughout the precipitate, then the atomic graph of the structure should have the following properties:

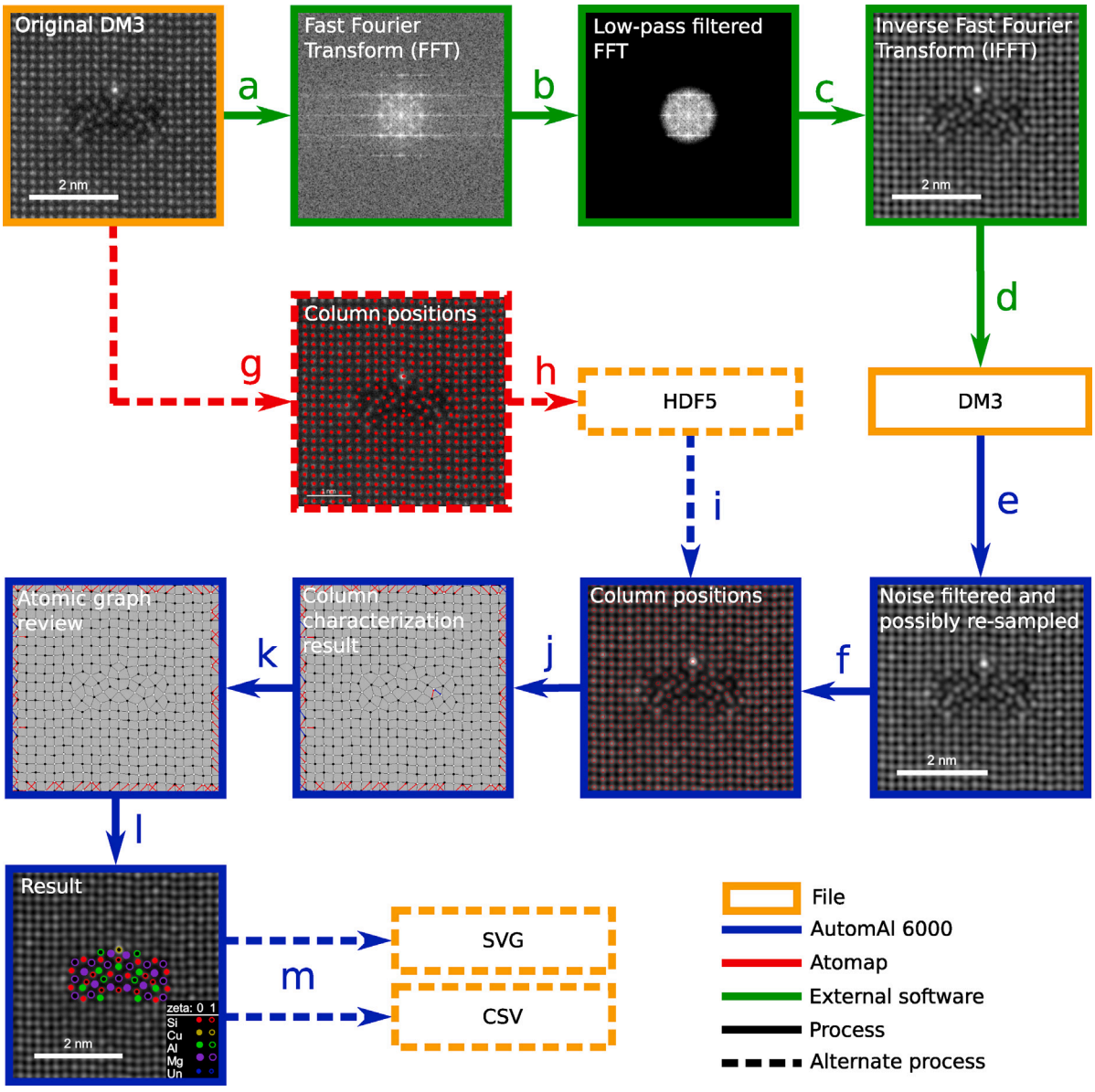

Fig. 3. Schematic of the AutomAl 6000 workflow. Column detection is performed with *atomap* [14], or by appropriate pre-processing, followed by AutomAl 6000's centre of mass column detection. The steps are; (a) import the image with software like for instance *gatan microscopy suite* (GMS) [15], and perform fast Fourier transform (FFT), (b) apply low pass mask on the FFT with a radius of approximately 6,7 nm^{-1}, (c) apply inverse FFT, (d) save results in the DM3 file format, (e) import DM3 file with AutomAl 6000, and (f) guess a threshold value and run column detection. Alternatively, (g) open image with atomap and perform column detection, (h) save result in the HDF5 file format and (i) import the HDF5 file into AutomAl 6000. Once column positions have been determined, precipitate characterization may be performed with the steps; (j) AutomAl 6000's column characterization algorithm, (k) manual corrections based on review of the atomic graph, (l) refresh statistics and finally, (m) export of the data, either as CSV for parsing the 3D positions and species into other software, or SVG for making high quality atomic overlays with any SVG software, for instance *Inkscape* [16].

Table 1
Overview of discussed graph edits. The logic notation $A \Rightarrow B$, reads "if A, then B", and $A : B$, reads "A, such that B". The assignment operator $A := B$, means to assign the evaluation of B to A. Entries marked with (*), are mostly used by the column characterization algorithm. Manual atomic graph review with the AutomAl 6000 GUI only supports the application of the unmarked entries, making them the important edits for a potential user of the software to know.

Edit	Notation	Effect	Strong
Arc pivot	$\widehat{P}_{ijk}(G)$	$(v_i v_j \in A(G) \wedge v_i v_k \notin A(G)) \Rightarrow (v_i v_j \rightarrow v_i v_k)$	No
Plane inversion	$\widehat{I}_i(G)$	$(\zeta_i = 0 \Rightarrow \zeta_i := 1) \vee (\zeta_i = 1 \Rightarrow \zeta_i := 0)$	No
Degree increment	$\widehat{D}_i^+(G)$	$(\deg^+(v_j) < 5) \Rightarrow (\deg^+(v_i) := \deg^+(v_i) + 1)$	Yes
Degree decrement	$\widehat{D}_i^-(G)$	$(\deg^+(v_i) > 3) \Rightarrow (\deg^+(v_i) := \deg^+(v_i) - 1)$	Yes
Weak arc preservation*	$\widehat{W}_{ij}^+(G)$	$k \Rightarrow \widehat{P}_{ikj}(G)$	No
Weak arc termination*	$\widehat{W}_{ij}^-(G)$	$k \Rightarrow \widehat{P}_{ijk}(G)$	No
Strong arc preservation*	$\widehat{S}_{ij}^+(G)$	$\widehat{D}_j^+(G) : (v_j v_i \in A(G))$	Yes
Strong arc termination*	$\widehat{S}_{ij}^-(G)$	$\widehat{D}_i^-(G) : (v_i v_j \notin A(G))$	Yes

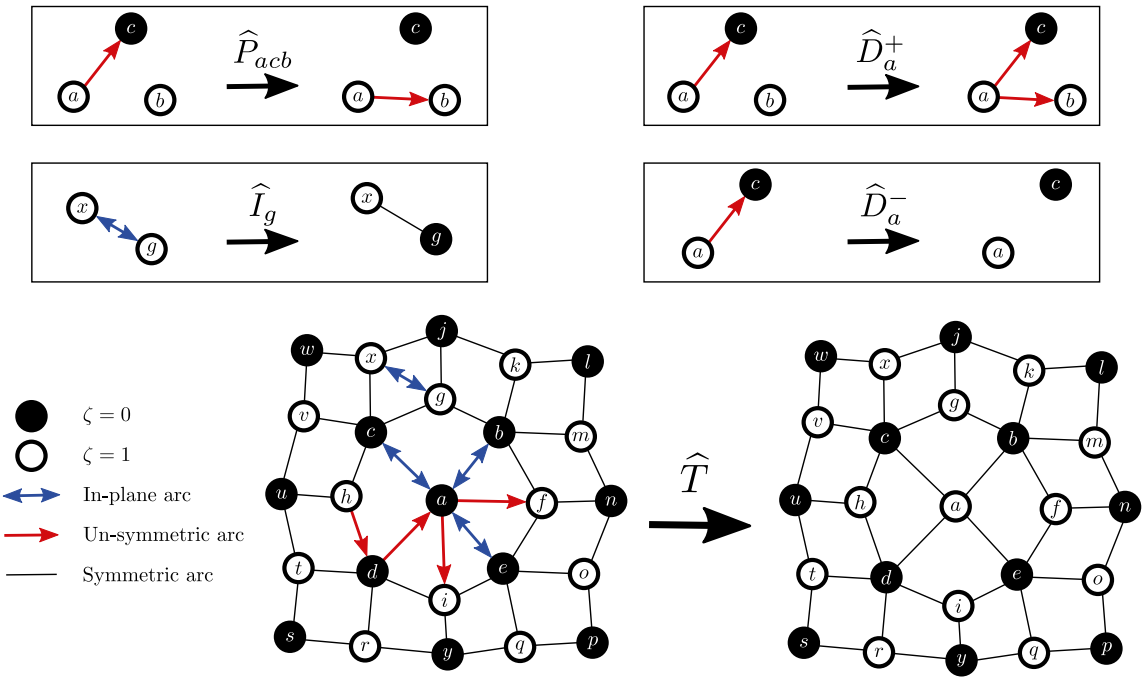

Fig. 4. Atomic graphs. Along the top of the figure, the effects of the most basic graph edits are illustrated: Arc pivot $\widehat{P}_{acb}$, plane inversion $\widehat{I}_g$, degree increment $\widehat{D}_a^+$ and degree decrement $\widehat{D}_a^-$. Below and to the right is the OPNN structure of a β'' eye represented with an atomic graph. On the left is the same structure with some erroneous parameters, which through the permutations $\widehat{T} = \widehat{I}_a + \widehat{S}_{xg}^- + \widehat{S}_{gx}^- + \widehat{S}_{hd}^+ + \widehat{S}_{af}^- + \widehat{P}_{aid}$, produces the correct graph.

1. For every vertex v_i, $\deg^+(v_i) \in \{3,\ 4,\ 5\}$.
2. For every arc $a_j = v_k v_l$, the component vertices belong to opposite planes such that $\zeta_k \neq \zeta_l$.
3. For every arc $a_j = v_k v_l$, the arc set must contain its inverse, that is, $v_k v_l \in A(G) \Rightarrow v_l v_k \in A(G)$, which implies that G is symmetric.
4. Arcs cannot intersect, given meaningful vertex positions in a 2D plane.
5. The number of vertex corners in any mesh is 4.

If the above properties hold, thus excluding the presence of dislocations, vacant positions and certain phases like β', then the average symmetric degree over the entire embedded precipitate becomes

$$\frac{1}{n}\sum_{i=1}^{n} \deg^{\leftrightarrow}(v_i) = 4. \tag{10}$$

This implies that in precipitates where the principles hold, the number of 3 OPNN column positions (Si or Cu), exactly matches the number of 5 OPPN column positions (Mg), while the number of 4 OPNN column positions (Al or 4-fold Cu) may vary.

2.2. Untangling

Untangling is one of the novel automated methods developed for AutomAl 6000, which seeks to resolve un-symmetric arcs (arcs that do not have inverse arcs) into symmetric arcs (having inverse arcs) in a way which produces an atomic graph that correctly represents the actual OPNN structure of the precipitate. Untangling reviews the local arc configurations around any un-symmetric arc and compares it to a library of pre-defined configurations to determine which graph edit to perform, if any. The particular library currently used is shown in Fig. 5. The details of this library are obtained by studying which configurations commonly appear by equating NN with vertex separation minimization. This library encodes a fine balance; it is possible to solve any graph by adding the appropriate configurations to the library, however, this could potentially produce erroneous results in other graphs or areas of graphs.

There are also two approaches for untangling, classified here as *strong* or *weak*, depending on whether altering vertex degrees are allowed or disallowed, respectively. Weak untangling is preferred, since strong untangling will sometimes compete or override the inferences of the statistical model. Once weak untangling is performed, only a few highly predictable subgraph configurations are subject to strong untangling.

2.3. Attributes

The numerical attributes considered for statistical inference are either graph angles which indicate OPNN symmetry, or Z-contrast which indicates column species. Fig. 6 explains how the α-angles are defined: Given the graph restriction $\deg^+(v_i) \in \{3,\ 4,\ 5\}$, choose[2] 3 vertices $\{v_j,\ v_k,\ v_l\}$ from $N^+(v_i)$ and find the angular separation in radians between vectors in the three pairs $v_i v_j$, $v_i v_k$ and $v_i v_l$. The resulting $\alpha_{\min}$ and $\alpha_{\max}$ are especially useful when atomic species, and therefore the appropriate out-degree of the vertex, are unknown. This is because by selecting the 3 OPNN of the vertex, an indication of the column symmetry is provided without *a priory* assumptions about the vertex degree. Note that there are two possible scenarios that can occur if $\deg^+(v_i) = 5$, leading to two separate distributions for Mg.

An additional consideration in the statistical classification scheme is the Z-contrast of the columns. The values of the pixels belonging to a concentric circular area[3] around each column centre are initially averaged. The peak value of the same set is also recorded, leading to two ways to measure the intensity (*avg* and *peak*). A subsequent normalization ensures that the average Z-contrast in the matrix (excluding the precipitate) is set to a predetermined value. This method will, to some degree, amend the problem of the considerable variation in absolute intensity from image to image, while preserving the relative intensity information. The *normalized average gamma* γ_{avg}, as well as

[2] In principle one could select 3 at random, but it is more effective to choose the 3 closest vertices in terms of the projected distances in the image plane.

[3] With radius $r \approx 1.0$ Å.

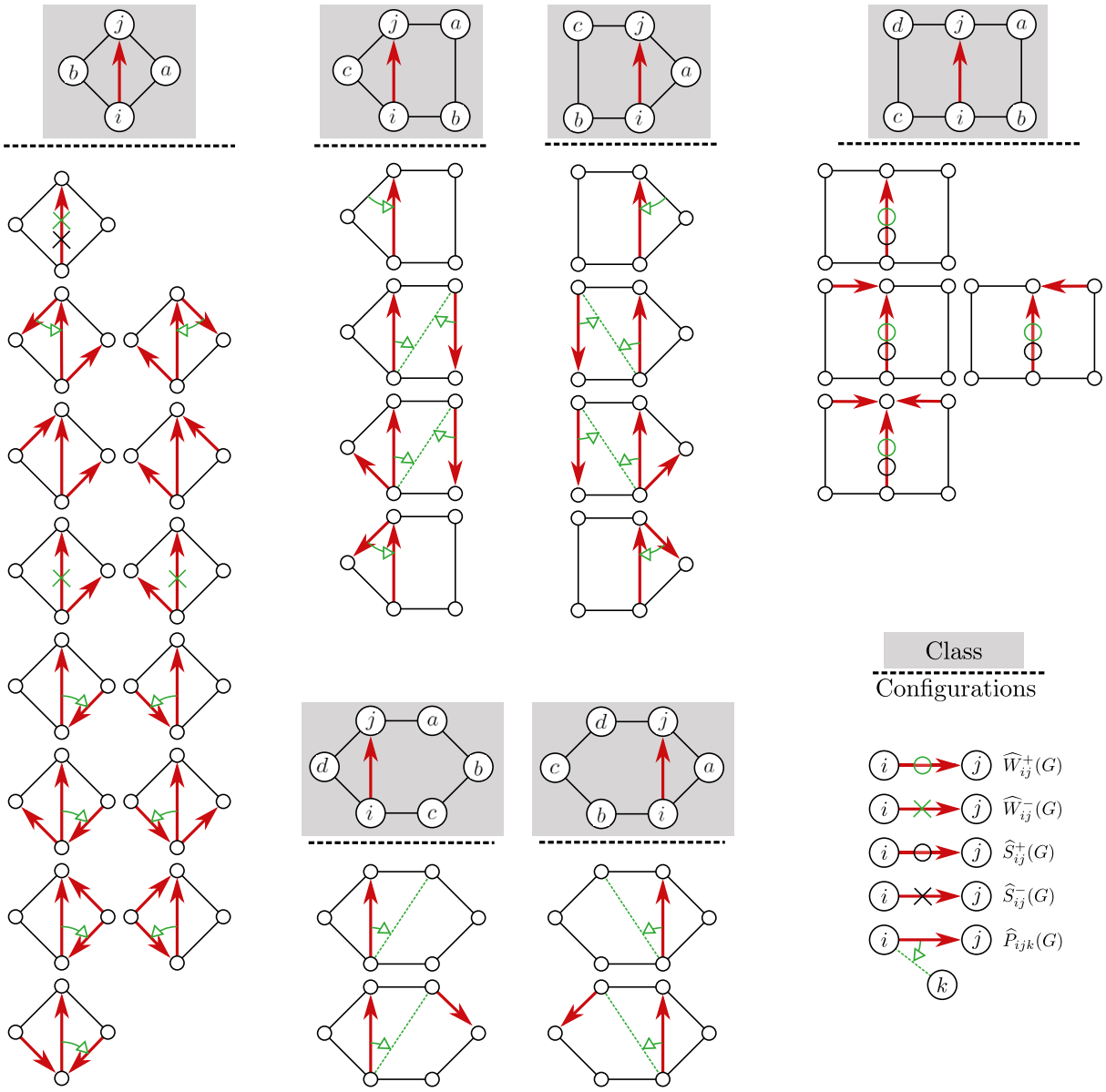

Fig. 5. Untangling library of arc centred sub graph configurations. Based on the local subgraph configurations centred on un-symmetric arcs in the atomic graph G, the untangling aims to permute arcs such that a more symmetric graph is approached. Which permutations are chosen depends on whether it is the strong (blue) or weak (green) untangling.

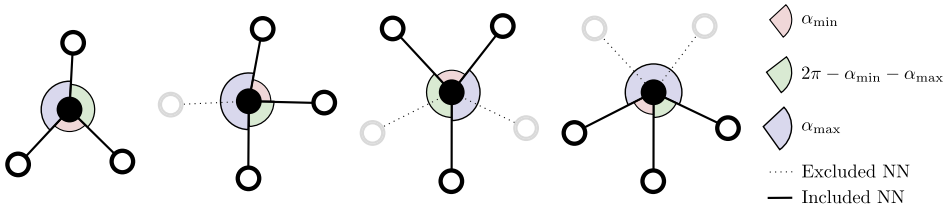

Fig. 6. Angle definitions. The α-angles are found by selecting the 3 nearest OPNN's and subsequently considering the angles between the arcs of those OPNN's. This figure shows the possible scenarios given that the vertex degree is either 3, 4 or 5.

the *normalized peak gamma* γ_{peak}, correlate with the dominant atomic species of the columns.

The numerical attributes $\alpha_{\min}$, $\alpha_{\max}$, γ_{avg} and γ_{peak} constitute a 4D space where multivariate normal distributions can be calculated from labelled data, which in turn can infer the atomic species on new unlabelled intensity data.

2.4. Default statistical model

Although the modelling scheme of AutomAl 6000 allows users to build custom models from own data, the default model is used to produce initial overlays, which are then corrected manually. A custom model can then be built from those overlays. The default model is

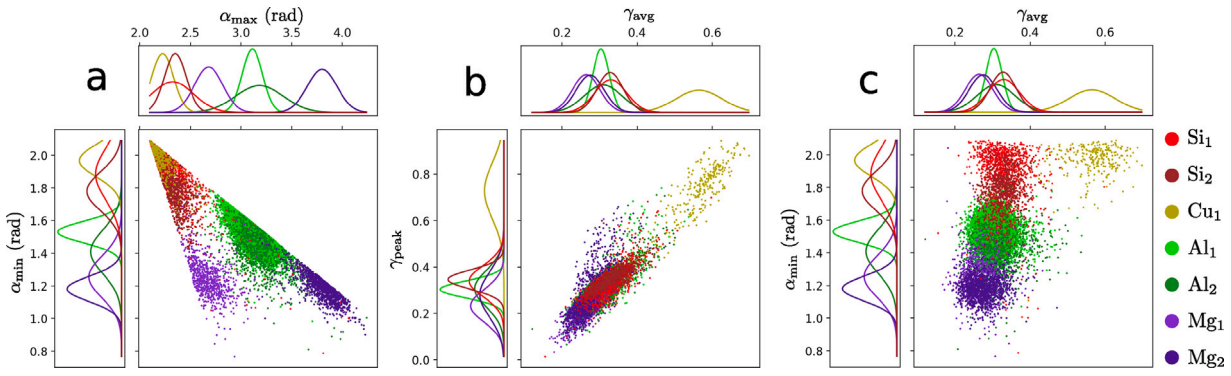

Fig. 7. Default model data. Shown here are 3 selected 2D projection planes through the same 4D data from a collection of fifteen HAADF-STEM images, which were used to calculate the default model parameters $\boldsymbol{\mu}_l$ and $\boldsymbol{\Sigma}_l$ for each category $s_l = \{\text{Si}_1, \text{Si}_2, \ldots \text{etc}\}$ (see Table 2). For each projection plane (a–c), both axes are supplemented with the single attribute normal distributions of the data projected onto each axis. Considering first the (a) α_{min} and α_{max} plane, it becomes clear why Mg needs to be considered with two different distributions as a consequence of the definition of the α-angles and the two possible scenarios that can occur when choosing 3 random vertices from the 5 available adjacent vertices of a Mg column. Plane (b) shows the γ_{avg} and γ_{peak} attributes. Here, the Cu_1 stands out from the other categories and illustrates how Cu can be identified by Z-contrast. Contrast alone is not sufficient for identifying the other categories well. However, the γ_{avg} and α_{min} plane (c) show how the main categories can be separated by combining Z-contrast information with OPNN symmetry information.

Table 2
Species dictionary of the default model, or the nominal attribute categorization scheme. Entries marked with (*) are not actually in the default model, but are provided to exemplify some categories which are natural to include in the species dictionary of certain images.

Adv. species	At. species	Out-degree	Description
Si_1	Si	3	Si found in β'' and interfaces.
Si_2	Si	3	Si found as in-plane NN to Cu in Q'.
Si_3*	Si	3	Interstitial Si in β'.
Cu_1	Cu	3	Cu with 3-fold NN symmetry.
Cu_2*	Cu	4	Cu with 4-fold NN symmetry.
Al_1	Al	4	Matrix Al.
Al_2	Al	4	Precipitate Al.
Mg_1	Mg	5	Mg with $\alpha_{\text{max}} \leq 3.12$.
Mg_2	Mg	5	Mg with $\alpha_{\text{max}} > 3.12$.
Un_1*	Un	3	A special *unknown* label.
Un_2*	Un	4	Vacancy column

constructed from data containing the phases β'', L, Q', β'_{Cu} and disordered precipitates, by using Eqs. (2) and (3). The nominal attribute has been termed *advanced species*, with the categories as presented in Table 2. Fig. 7 shows the data points projected onto three different 2D planes through the 4D attribute space. For each axis, the 1D normal distribution of the data in the relevant attribute, is also shown. This visualization of the data provides some indication of how the data clusters. Note that when combining Z-contrast, represented by γ_{avg}, with symmetry, for instance α_{min}, the best cluster separation of the model is visualized, as in Fig. 7c. There is some overlap between the clusters, which is a limiting factor in the accuracy of the column characterization algorithm approach in this work.

2.5. ζ-analysis

Determining the Boolean ζ_i-value of each vertex v_i is an integral part of the problem, that is, determining which of the two planes each column belongs to. To achieve this, a method which lets all vertices vote on the plane association of their OPNN was conceived and consequently termed ζ-*analysis*.[4]

Consider a seed vertex v_s that is originally given a vote $V_s^0 = 1$, while all other vertices in the graph G are given a vote of 0, such that

$$V_i^0 = \begin{cases} 1 & \text{if } i = s \\ 0 & \text{if } i \neq s. \end{cases} \tag{11}$$

Next, define two parameters $w_1 \in (0, 1)$ and $0 \leq w_2 < w_1$. Formally, for each election cycle $c = \{0, 1, \ldots, C-1\}$, and for each $i \in \{1, 2, \ldots, n\}$, where n is the order of the graph, set

$$V_i^{c+1} = V_i^c - w_1 \sum_{j \in X} V_j^c - w_2 \sum_{k \in Y} V_k^c, \tag{12}$$

where X is the set of all indices j such that $v_j \in P(v_i)$, and Y is the set of all indices k such that $v_k \in N^-(v_i) - P(v_i)$. In addition, limit $V_i^{c+1} \in [-100, 100]$ with

$$V_i^{c+1} := \min\left[100, \max\left[-100, V_i^{c+1}\right]\right], \tag{13}$$

so as to prevent explosive growth from positive feedback loops which will appear over symmetric arcs. To illustrate, consider a graph that is fully symmetric, which implies that Y is empty. In the first election cycle, given that all $V_{i \neq s}^0 = 0$, it is only the partners of the seed vertex $\{v_p\} = P(v_s)$ who will have their votes increased to

$$\begin{aligned} V_p^1 &= \min\left[100, \max\left[-100, V_p^0 - w_1 \sum_{j \in X} V_j^0\right]\right] \\ &= -w_1. \end{aligned} \tag{14}$$

This means that in the second election cycle, the seed vertex vote increases to

$$\begin{aligned} V_s^2 &= \min\left[100, \max\left[-100, V_s^1 - w_1 \sum_{j \in X} V_j^1\right]\right] \\ &= 1 + \deg^{\leftrightarrow}(v_s) w_1^2, \end{aligned} \tag{15}$$

which therefore further increases v_s. This illustrates how positive feedback occurs over symmetric arcs, minimizing the influence of unsymmetric arcs as the voting spreads across the graph over many election cycles, maintaining all voting relative to the seed vertex, which is therefore acting as a source. After a sufficient number of election cycles ($C \sim 0,05n$), all V_i will converge to a value of 100 or -100, which is then used to set

$$\zeta_i = \begin{cases} 1 & \text{if } V_i^C \geq 0 \\ 0 & \text{if } V_i^C < 0, \end{cases} \tag{16}$$

and thus set the z_i-positions of each vertex by using Eq. (7).

The implementation of this method in AutomAl 6000 also features additional sophistication to prevent edge effects from the graph edges by defining a third weight $w_3 < w_2$, which replaces either w_1 or w_2 if the corresponding vertex is an edge vertex. Furthermore, the ζ-analysis is first applied to the Al matrix, before the precipitate is analysed by using the precipitate interface columns as 'seeds'. The

[4] Not to be confused with other general uses of the term *zeta analysis* in both material science and mathematical literature. The method discussed here is original to the best of our knowledge.

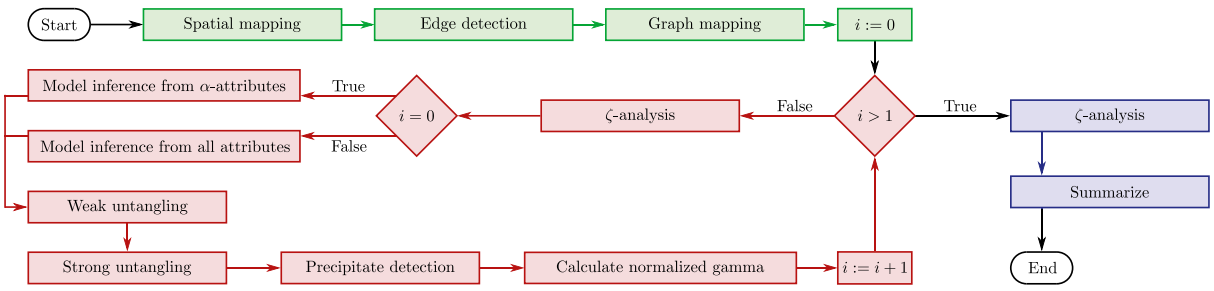

Fig. 8. Column characterization algorithm. The AutomAl 6000 column characterization algorithm represented as a flow-chart. The algorithm relies on multiple sub-processes distributed between an initialization part (green), a recurring part (red) and a finalization part (blue). The individual sub-processes themselves, as well as the order in which they are applied, can influence the result of the algorithm. The sub-processes are detailed in the text.

current implementation uses

$$\begin{aligned} w_1 &= 0,5 \\ w_2 &= 0,2 \\ w_3 &= 0,1. \end{aligned} \tag{17}$$

2.6. Spatial mapping and graph mapping

The *projected separation* Δ' between any two vertices v_i and v_j is the distance between the vertices in the image plane

$$\Delta'(v_i,\ v_j) = \sqrt{(x_j - x_i)^2 + (y_j - y_i)^2}. \tag{18}$$

The projected separations between all vertices are used to establish a general locality for each vertex and to map the initial arc set from the vertex set. The *projected separation matrix* $\boldsymbol{M}$, is therefore calculated with elements

$$M_{ij} = M_{ji} = \Delta'(v_i,\ v_j). \tag{19}$$

Once $\boldsymbol{M}$ is calculated, every vertex is labelled as Un_1, which dictates that the out-neighbourhoods should contain 3 vertices, as per Table 2, which, for vertex v_a, will be the vertices corresponding to the indices $\{b\}$ of the 3 smallest values in row $M_{a\{b\}}$, excluding $b = a$. This provides the initial atomic graph mapping, where OPNN are thus simply assumed to be the 3 nearest vertices.

2.7. Edge and precipitate detection

The algorithm does not account for vertices at the edge of the graph, so columns near the edge of the image are labelled accordingly, and disregarded from further study.

Another task for the algorithm is to determine which columns are part of the precipitate or which columns are part of the aluminium matrix. This is achieved by defining every aluminium column with 1 or 0 non-aluminium OPNN as matrix columns, and all other columns as precipitate columns. The more accurate the labelling is, the more accurate the precipitate detection is, which is why this part is included in the recurring part of the algorithm. Distinguishing the precipitate from the matrix is important to get appropriate normalized γ-attributes, as well as an estimate of the composition of the precipitate.

2.8. Column characterization algorithm

The full column characterization algorithm featured in AutomAl 6000, consists of all the methods discussed above, applied in a certain order. Both the implementation details of the individual methods as well as the eventual sequence of the methods will influence the result of the algorithm. The involved parts, as well as their order, are illustrated in Fig. 8. The algorithm has three parts: An initialization part, a recurring part and a finalization part. In Fig. 8, these parts are indicated with green, red and blue, respectively. During the initialization, basic properties of the column arrangement are extracted, which is only done once. In the recurring part, the statistical model and the untangling are applied alternately, in theory improving each cycle until converging at a static state. In practice however, this convergence happens already after a few repetitions, so any convergence testing is replaced by a simple repetition count. This is discussed further in the discussion section. The finalization part assumes that an optimal graph symmetry has been set, and uses this to perform the most optimal ζ-analysis. It will also summarize all data to make sure all object fields and attributes are up to date.

Although the details of the algorithm are always subject to change and improvements, there are some basic concepts that inform some of the sequencing decisions of the algorithm design. For instance, when $i = 0$, it is unknown if columns are part of the matrix or the precipitate, so a proper γ-normalization cannot be calculated. Therefore, it is more accurate to use only α-angles when applying the statistical model. Untangling should also immediately follow the model inference, and ζ-analysis should always be performed after precipitate detection, except when $i = 0$.

3. Results and discussion

We demonstrate the application of the AutomAl 6000 method on three different HAADF-STEM images of Al–Mg–Si(–Cu) precipitates as presented in Fig. 9. The images were selected to give a representation of the range of images that AutomAl 6000 is designed for. An image- and probe corrected JEOL ARM200CF microscope operated at 200 kV was used to acquire the images. For the acquisition, the convergence angle was 27 mrad, while the inner and outer detector collection angle were 35 mrad and 149 mrad, respectively. Alloy details are provided in Table 3. For each of the images, a *control overlay* was produced manually, which (to the best of knowledge) represents the correct atomic overlay. AutomAl 6000 has been found to identify the column species with high precision, as summarized in Table 4, where the errors compared to the manual control overlays are given. Note however, that the errors only relate to the initial characterization, which are reduced by a manual atomic graph review, which is an elementary part of the AutomAl 6000 process. This manual atomic graph review is exemplified in the next section, before some additional highlights from the development of AutomAl 6000 are discussed.

3.1. Manual atomic graph review

Fig. 10 shows the resulting atomic graph after applying the column characterization algorithm on an image. Fig. 10 also features enlarged areas of the graph, with some vertices arbitrarily labelled, and with the graph edits required to solve the atomic graph provided in the figure description. Once the correct OPNN structure is acquired, atomic species with the same associated out-degree, should also be controlled, since these will appear identical in the atomic graph. In the Al–Mg–Si–Cu system, this will involve checking that the Cu and Si columns are

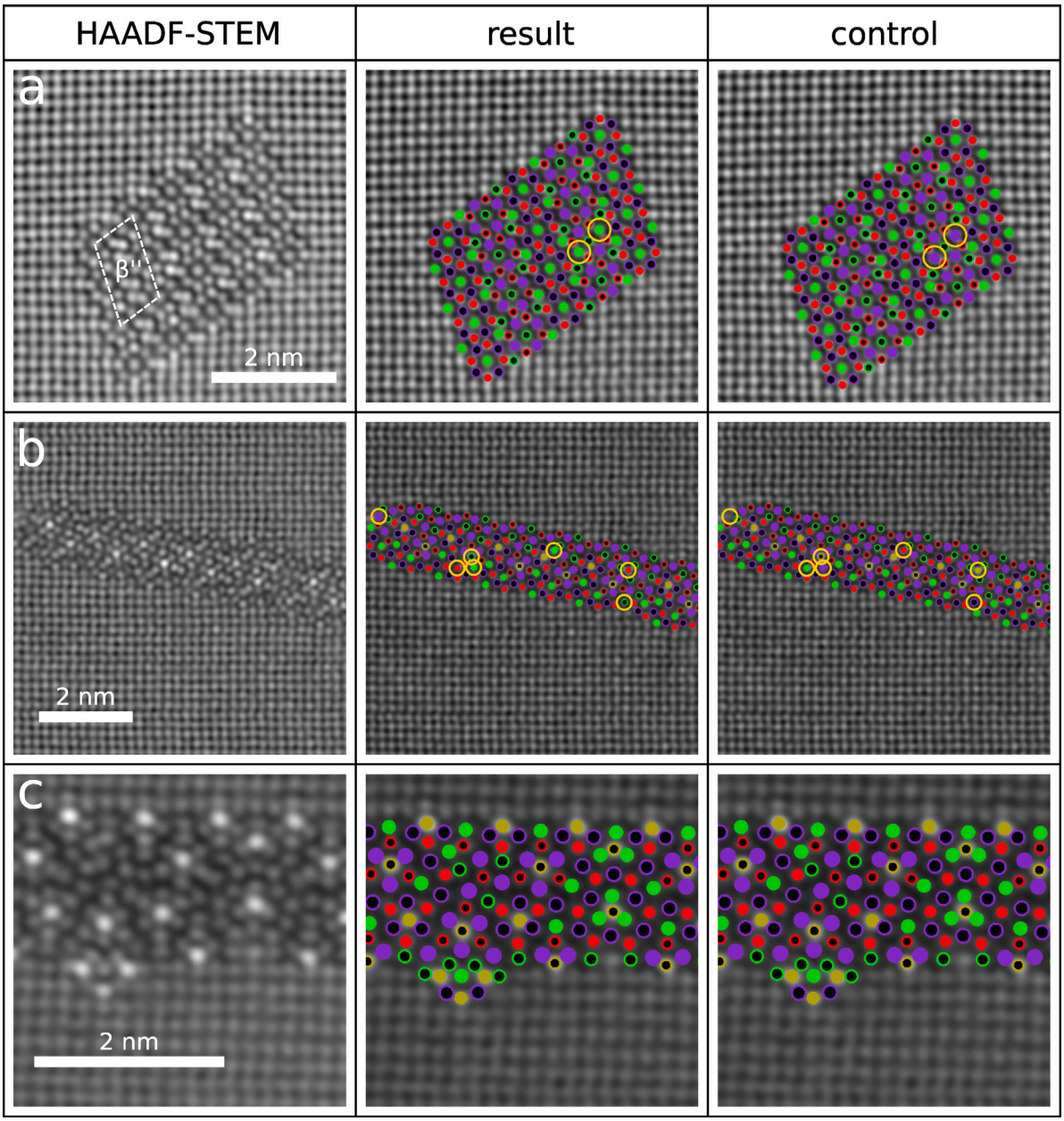

Fig. 9. Example HAADF images of 3 different precipitates in [001]Al zone. The left column shows sections of the HAADF-STEM images chosen for this study: (a) β'' precipitate, (b) Q' precipitate, and (c) L precipitate which also features a β'_{Cu} unit. Image details can be found in Table 3. Middle column shows the result of the column characterization algorithm, without any manual graph review, and the right column shows control overlays. The discrepancies between the result and control overlays are highlighted by yellow circles. For overlay legend, see Fig. 1. For relative discrepancies, confer Table 4.

correctly labelled. Following the structural principles and manipulating the atomic graphs accordingly, might take some effort getting used to, but is essential for understanding the full AutomAl 6000 process, as the error percentage of the algorithm may vary based on the particulars of individual images.

3.2. Algorithm convergence

To test the general behaviour of the column characterization algorithm, a set of 12 varied images[5] with known control overlays are used. Fig. 11 shows the results of such a test, where by applying the algorithm on each image and comparing with the control image at each step, a reliably converging trend is seen. The error that the algorithm converges to, will vary slightly between images depending on details of the image and/or the structure of the precipitate, but is generally expected to be low. On the 12 images in the test set, the average difference at $i = 4$ was $2,9\%$, with a standard deviation of $2,3\%$. The vertical lines in Fig. 11 indicate iterations of i, starting with $i = 0$ at the leftmost stippled line (the initialization part of the algorithm is not shown as the error is always 100 percent until the first model inference). Although some small improvements are sometimes observed

[5] The specific images used for this test are not provided with this paper, as they appear in other works. It can however be stated that the set includes images from different TEM sessions with different acquisition parameters, and a wide range of precipitate sizes, alloy compositions and structural content, like β'', β'_{Cu}, Q', L, disorder and hybrid particles.

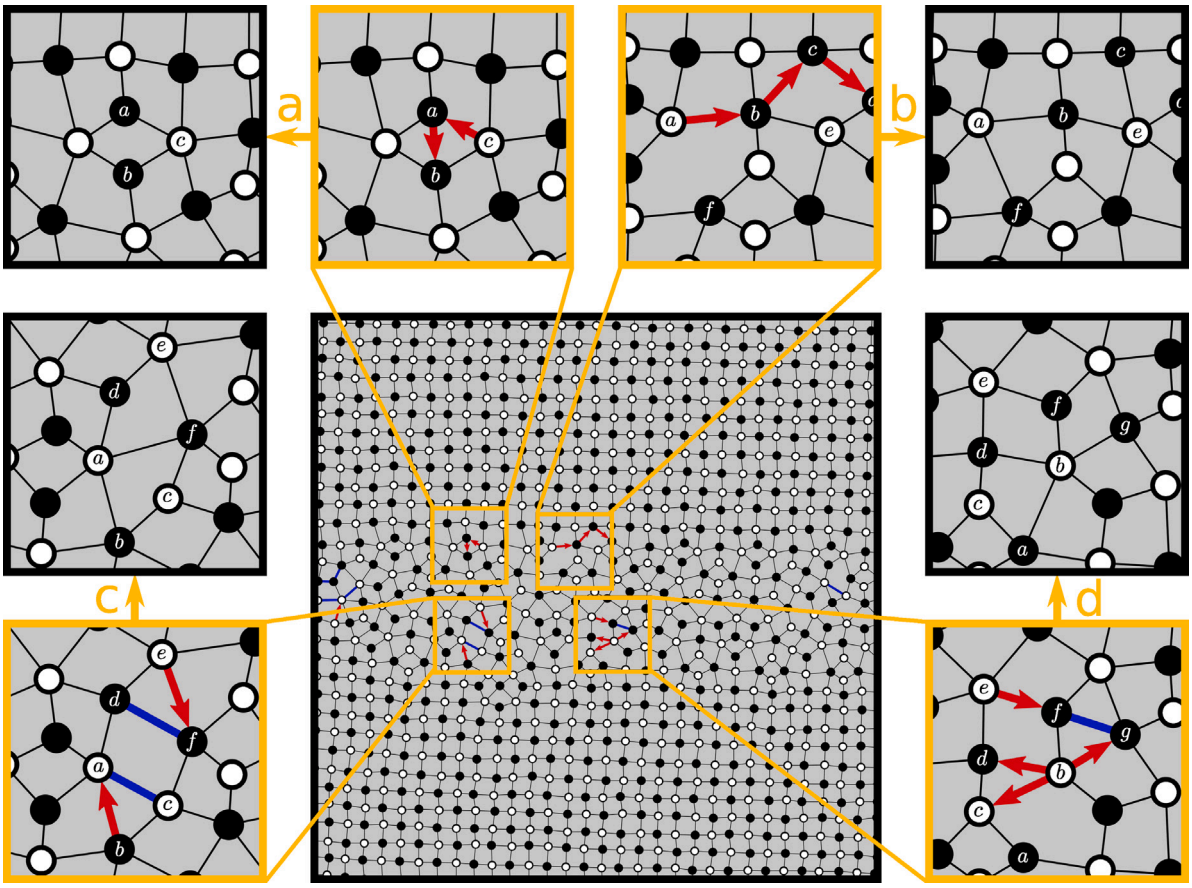

Fig. 10. Atomic graph review. The central panel shows the atomic graph of the column characterization result of an image. The four highlighted areas of the atomic graph featuring un-symmetric arcs indicate that manual review is necessary. By following the structural principles as expressed in graph properties, one can arrive at the following edit sequences to solve the OPNN structure of these areas; (a) $\hat{P}_{abc}$, (b) $\hat{P}_{bca} + \hat{P}_{cda} + \hat{S}^{+}_{ce} + \hat{S}^{+}_{fa} + \hat{S}^{+}_{af}$, (c) $\hat{P}_{fde} + \hat{P}_{acb} + \hat{S}^{-}_{ca} + \hat{S}^{-}_{df} + \hat{S}^{+}_{fa} + \hat{S}^{+}_{af}$ and (d) $\hat{P}_{gfb} + \hat{P}_{fge} + \hat{P}_{bca} + \hat{S}^{+}_{bd} + \hat{S}^{+}_{ba}$. The key when trying to find the correct edits during manual atomic graph review, is to notice the number of corners in each mesh, which should be 4 if the structural principles are valid in the area being considered (which, as discussed above, is normally the case).

after $i = 2$, these are considered minor and the algorithm is terminated at $i = 2$ to optimize run time.

3.3. Insights provided by the default model data

Fig. 7 illustrates an organization of the data that can provide useful information: Fig. 7b shows the expected linear relation between the normalized γ_{peak} variable (the brightest pixel value within each column radius), and the normalized γ_{avg} variable (the average pixel value within each column radius). However, a group of Mg columns located in a bulge extending upwards from the main clustering, deviates slightly from this relation. Upon closer inspection, they were identified as Mg columns which are also OPNN columns to Cu in Q′ phases. They will have both inflated average and peak pixel values, with the effect most prominent in the peak pixels values. This is because their positions are biased towards the much brighter Cu when using AutomAl 6000's centre of mass column detection, due to the intensity of the Cu columns slightly bleeding into the neighbouring columns. The effect is a displacement of such Mg columns to positions nearer the Cu columns, with a resulting bleeding effect and inflated pixel values of Mg, which again makes them stand out in the γ-plane. A similar bias can be seen with Al columns which have a OPNN relation to Cu in β'_{Cu}.

Another point of interest is the slight shift in the mean values of the distributions of Cu, Si_1 and Si_2 in the α_{min} variable. They are all 3 OPNN column positions, but the Cu distribution mean is visibly closer to the value representing perfectly symmetric triangular positions, while Si_1 will typically occupy structural positions that are more skewed away from symmetry, and Si_2 even more so. This can be explained by the fact that in the Q′ and β'_{Cu} phases, Cu inhabit positions surrounded by three symmetrically indistinguishable neighbour positions. In contrast, Si_2 in a same plane NN relation to these Cu positions is in a lower symmetry position regarding the 3 OPNN positions with 2 Mg and 1 Al columns [18]. This illustrates how different local column configurations and symmetry can be interpreted from visualizations by the program.

3.4. Effects of image quality

It is important to consider the effect of overall image quality. In the presence of heavy atom species resulting in bright columns, e.g. Cu or Zn, a cut-off in the histogram is to be expected for long dwell times, commonly known as over-saturation. To increase the precision it is advantageous to stay within the dynamic range of the detector, if possible in the linear range, and avoid over-saturation. In this way, the column intensity can be more accurately assigned to a specific element and the natural scatter range of different intensities will be minimized together with the variance of the γ_{avg} distributions as per Fig. 7b. In the long run, this will aid discrimination of the different atom species with closely related Z-numbers.

Additional parameters for image quality are the condenser aperture radius and inner detector radius. The condenser aperture should be chosen as large as possible while still excluding lens aberrations to get the best image resolution. The most straight forward interpretable Z-contrast images are achieved when inter and intra columnar interference effects can be excluded [19]. Hartel et al. [20], showed that for cubic crystals with lattice constants $\propto 0.4$ nm, this can be achieved to a large extend by imaging with an inner detector collection angle of $\Theta_1 = 50$ mrad.

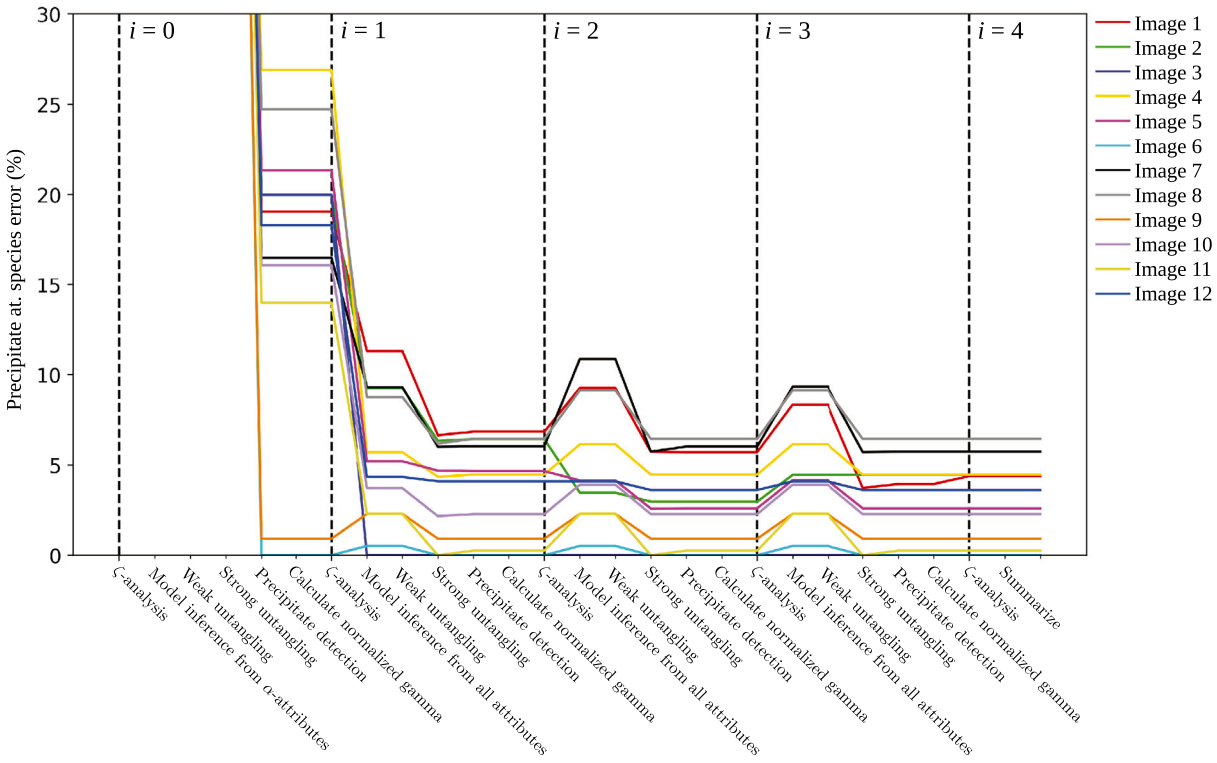

Fig. 11. Column characterization algorithm convergence behaviour. This graph shows the precipitate atomic species error in percent after each individual algorithm step over a set of 12 varied images. The vertical stippled lines indicate the iterations of i, as per Fig. 8, which in this test is allowed to exceed $i = 2$. After the first application of precipitate detection, the error drops down dramatically the first time the precipitate error can be measured. Subsequent application of precipitate detection, gamma normalization, weak untangling and ζ-analysis have no effect on error: These methods do not affect the identification atomic species directly, but usually influence how the statistical labelling perform. The error changes after statistical labelling and strong untangling, as these are the only methods that alter atomic species labels. The error is often seen to increase with the model inferences, but this allows weak followed by strong untangling to further decrease the error, unless the convergence error has been reached.

Table 3
Image details of Fig. 9. Alloy treatment consist of: Solution heat treatment (SHT), water quench (WQ), natural ageing (NA), artificial ageing (AA) and direct artificial ageing (DAA).

Image	Alloy (at%)	Alloy treatment	Features
a	0.63Mg, 0.62Si, 0.06Cu, 0.08Mn, 0.10Fe	SHT + WQ + 2 h NA + 2 h AA @ 185 °C.	β''
b	0.63Mg, 0.62Si, 0.06Cu, 0.08Mn, 0.10Fe	SHT + WQ + 2 h NA + 20 h AA @ 150 °C.	Q′
c	1.20Mg, 0.37Si, 0.20Cu	SHT + WQ + 64 min DAA @ 250 °C.	L and β'_{Cu}

Table 4
Error results of the column characterization algorithm applied on images a–c in Fig. 9. Calculated as the number of erroneous atomic species labels in the precipitate, divided by the number of columns in the precipitate, and scaled by 100 to produce a percentage.

Image	Error (%)
a	0,92
b	2,28
c	0,25

4. Conclusions

The stand-alone software AutomAl 6000 is used to analyse HAADF-STEM images of precipitate cross-sections in the Al-Mg-Si-(Cu) system and returns the atomic structure with high accuracy. The novel algorithm combines a statistical model with a set of simple structural principles relating columns of the aluminium and the solutes. The software allows for rapid,[6] determination of the entire 3D atomic structure responsible for the 2D precipitate/matrix cross-section projection with minimal manual input, demonstrating that the structural principles represent fundamental simplifying generalizations of the precipitates in this system, which can aid materials development. The software allows for more quantitative studies of these alloys, and provides an excellent starting point for making SVG atomic overlays for both researches and students. Such overlays are produced with layered species information in the SVG metadata, which may have a broader use than discussed in this paper. The software is open source and available to anyone from the links provided in the abstract.

The implementation of the data structure of AutomAl 6000 is fairly general, and even without the column characterization, can be used to manually characterize novel data to acquire the distribution of different physical attributes in a structure. The relational character of the atomic graphs provides a capable basis for data analysis of precipitates, and might be employed to create large sets of labelled data intended for supervised machine learning techniques.

[6] For comparison, manual overlay of image b in Fig. 9 took 54 min (3 min for column detection, and 51 min for column determination using the AutomAl 6000 manual interface), while the same image analysed with AutomAl 6000 by a user familiar with atomic graphs, took 10 min (3 min for column detection, 5 min running column characterization and 2 min reviewing the atomic graph).

The approach that was taken with the column characterization algorithm in this work, relies heavily on two major facts about the precipitate system under consideration: (1) Every atomic species present in the system are significantly separable along at least one direction in the parameter space, as in Fig. 7c. (2) There are unambiguous and known structural principles present, which can be correctly interpreted by weak and strong untangling methods. Similar methods to those discussed in this work, but for different precipitate systems, can be feasible if the above facts are valid in the system.

4.1. Further work

The program will be tested on the precipitates growing on dislocations. This appears to be more common in the 2xxx system (Al–Mg–Cu), but with precipitates which use similar structural principles (column rules). Without modification, the rules may apparently break down on one side of the interface of precipitates growing on dislocations. It is yet unclear how this will require a modification of the algorithm. Further work will also include the alloys of the 7xxx system (Al–Mg–Zn). In these alloys the <100>Al columns are less important. Instead, plate-like precipitates take advantage of other rules. If this system can be tackled, the plan is to investigate how the description of other alloy systems can be simplified.

Declaration of competing interest

The authors declare that they have no known competing financial interests or personal relationships that could have appeared to influence the work reported in this paper.

Acknowledgements

This work was supported by the KPN projects ‘FICAL’ (Research Council of Norway (NFR):247598) (H.T), co-financed by Research Council of Norway (NFR), and the industrial partners Hydro, Gränges, Benteler Automotive Raufoss AS and Steertec Raufoss, and SumAl (NFR: 294933) (C.H. and R.H. supported by Hydro, Benteler Automotive Raufoss AS and Neuman Aluminium. In addition, the NTNU Digital Transformation initiative ‘Alldesign’ (E.T. and R.H.) has supported this work. The HAADF-STEM work was conducted on the NORTEM (Research Council of Norway (NFR):197405) infrastructure at the TEM Gemini Centre, Trondheim, Norway.

References

[1] S.J. Pennycook, P.D. Nellist, Scanning Transmission Electron Microscopy, first ed., Springer-Verlag GmbH, 2011, http://dx.doi.org/10.1007/978-1-4419-7200-2.

[2] D.B. Williams, C.B. Carter, Transmission Electron Microscopy: Diffraction, Imaging, and Spectrometry, Springer, 2016.

[3] M. Tisza, I. Czinege, Comparative study of the application of steels and aluminium in lightweight production of automotive parts, Int. J. Lightweight Mater. Manuf. 1 (4) (2018) 229–238, http://dx.doi.org/10.1016/j.ijlmm.2018.09.001.

[4] T. Saito, E.A. Mørtsell, S. Wenner, C.D. Marioara, S.J. Andersen, J. Friis, K. Matsuda, R. Holmestad, Atomic structures of precipitates in Al–Mg–Si alloys with small additions of other elements, Adv. Energy Mater. 20 (7) (2018) 1800125, http://dx.doi.org/10.1002/adem.201800125.

[5] S.J. Andersen, C.D. Marioara, J. Friis, S. Wenner, R. Holmestad, Precipitates in aluminium alloys, Adv. Phys. X 3 (1) (2018) 1479984, http://dx.doi.org/10.1080/23746149.2018.1479984.

[6] C.D. Marioara, S.J. Andersen, H.W. Zandbergen, R. Holmestad, The influence of alloy composition on precipitates of the Al-Mg-Si system, Metall. Mater. Trans. A 36 (3) (2005) 691–702, http://dx.doi.org/10.1007/s11661-005-0185-1.

[7] C.D. Marioara, S.J. Andersen, T.N. Stene, H. Hasting, J. Walmsley, A.T.J.V. Helvoort, R. Holmestad, The effect of cu on precipitation in Al–Mg–Si alloys, Phil. Mag. 87 (23) (2007) 3385–3413, http://dx.doi.org/10.1080/14786430701287377.

[8] C.D. Marioara, H. Nordmark, S.J. Andersen, R. Holmestad, Post-β phases and their influence on microstructure and hardness in 6xxx Al-Mg-Si alloys, J. Mater. Sci. 41 (2) (2006) 471–478, http://dx.doi.org/10.1007/s10853-005-2470-1.

[9] W.P. Davey, Precision measurements of the lattice constants of twelve common metals, Phys. Rev. 25 (6) (1925) 753–761, http://dx.doi.org/10.1103/physrev.25.753.

[10] S.J. Andersen, C.D. Marioara, J. Friis, R. Bjørge, Q. Du, I.G. Ringdalen, S. Wenner, E.A. Mørtsell, R. Holmestad, T. Saito, J. Røyset, O. Reiso, Directionality and column arrangement principles of precipitates in Al-Mg-Si-(Cu) and Al-Mg-Cu linked to line defect in Al, Materials Science Forum 877 (2016) 461–470, http://dx.doi.org/10.4028/www.scientific.net/msf.877.461.

[11] R. Vissers, M. van Huis, J. Jansen, H. Zandbergen, C. Marioara, S. Andersen, The crystal structure of the $\beta\prime$ phase in Al–Mg–Si alloys, Acta Mater. 55 (11) (2007) 3815–3823, http://dx.doi.org/10.1016/j.actamat.2007.02.032.

[12] A. Afifi, S. May, V.A. Clark, Practical Multivariate Analysis, Taylor & Francis, Boca Raton, 2012.

[13] G. Chartrand, L. Lesniak, P. Zhang, Graphs and Digraphs, sixth ed., CRC Press, 2016.

[14] M. Nord, P.E. Vullum, I. MacLaren, T. Tybell, R. Holmestad, Atomap: a new software tool for the automated analysis of atomic resolution images using two-dimensional Gaussian fitting, Adv. Struct. Chem. Imaging 3 (1) (2017) http://dx.doi.org/10.1186/s40679-017-0042-5.

[15] Digital Micrograph, Gatan, inc, URL https://www.gatan.com/products/tem-analysis/gatan-microscopy-suite-software.

[16] Inkscape, URL https://inkscape.org/.

[17] T. Cormen, Introduction to Algorithms, 2, MIT Press, 2001, pp. 527–531.

[18] T. Saito, C.D. Marioara, S.J. Andersen, W. Lefebvre, R. Holmestad, Aberration-corrected HAADF-STEM investigations of precipitate structures in Al–Mg–Si alloys with low Cu additions, Phil. Mag. 94 (5) (2013) 520–531, http://dx.doi.org/10.1080/14786435.2013.857051.

[19] D.E. Jesson, S.J. Pennycook, Incoherent imaging of thin specimens using coherently scattered electrons, Proc. Math. Phys. Sci. 441 (1993) 261–281.

[20] P. Hartel, H. Rose, C. Dinges, Conditions and reasons for incoherent imaging in STEM, Ultramicroscopy 63 (2) (1996) 93–114, http://dx.doi.org/10.1016/0304-3991(96)00020-4.